UKAEA FUS 459

EURATOM/UKAEA Fusion

On the possibility of inducing strong plasma convection in the divertor of MAST

D.D. Ryutov[a)], P. Helander[b)] and R.H. Cohen[a)]

June 2001

EURATOM/UKAEA fusion Association

[b)]Culham Science Centre, Abingdon
Oxfordshire, OX14 3DB
United Kingdom
Telephone +44 1235 463546
Facsimile +441235 463435

[a)]Lawrence Livermore National Laboratory
Livermore 94551
USA

On the possibility of inducing strong plasma convection in the divertor of MAST

D.D. Ryutov[a)], P. Helander[b)] and R.H. Cohen[a)]

[a)]Lawrence Livermore National Laboratory, Livermore, 94551, USA
[b)]EURATOM/UKAEA Fusion Association, Culham Science Centre, Abingdon, Oxfordshire, OX14 3DB, UK

In this paper, theory is developed to describe (SOL) broadening by inducing convective cells through divertor plate biasing in a tokamak. The theory is applied to the Mega-Ampere Spherical Tokamak (MAST), where such experiments are planned in the near future. Criteria are derived for achieving strong broadening and for exciting shear-flow turbulence in the SOL, and these criteria are shown to be attainable in practice. It is also shown that the magnetic shear present in the vicinity of the X-point is likely to confine the potential perturbations to the divertor region below the X-point, leaving the part of the SOL that is in direct contact with the core plasma intact. The current created in the SOL by the biasing and the associated heating power are also calculated and are found to be modest.

1. Introduction

In this paper, we discuss scrape-off layer (SOL) convection induced by electric biasing of the divertor tiles in a tokamak. This was suggested in Refs. 1 and 2 as a means to increase the SOL thickness and thereby reduce the heat load on the divertor. At present, such experiments are planned on the Mega-Ampere Spherical Tokamak (MAST) at Culham [3]. For the conditions present in MAST and other tokamaks with a poloidal divertor, it may be possible to limit the zone where the convection is present to the divertor legs. Potentially, this is the most desirable way of controlling transport in the SOL region. Indeed, if the induced convection is limited to the divertor legs, the cross-field transport on the open field lines above the X-point (Fig. 1) will remain the same as without any convection. This, in turn, means that there should be no direct effect of the induced convection on the plasma parameters above the X-point, either in the SOL or in the core. Some indirect effect may be caused by a rapid convective SOL broadening below the X-point but, in terms of the effect on the SOL above the X-point, this would at most be equivalent to moving the absorbing surface from the divertor floor to the X-point, with the corresponding reduction of the connection length. As in most divertor designs divertor legs are short compared to the total plasma circumference, this effect should be relatively insignificant. Therefore, we expect that, by exciting convection only

in divertor legs would allow one to increase the area of the wetted zone on the divertor plates without any significant confinement degradation of the core plasma.[1]

Electric biasing of the divertor tiles may not be the most practical way for the SOL broadening in the fusion reactor because of the possible degradation of insulators under intense neutron irradiation. On the other hand, the plasma physics effects related to this method of inducing the SOL convection are very similar to the corresponding effects in the other methods of inducing SOL convection (e.g., by toroidally asymmetric gas-puff, or by introducing toroidal waviness of the divertor floor [1, 2]). So, the successful realization of the proposed experiments on the MAST facility would shed light on the prospects of these other methods, whose implementation in the reactor environment is more straightforward.

The purpose of this paper is to develop the basic theory of induced SOL convection presented in Refs 1 and 2 to a point where it can be straighforwardly applied to an actual experiment, and in particular the one planned on MAST. Although our discussion is focused on MAST, most of the issues we discuss are not specific to this particular device and would be of importance in any tokamak where such experiments were performed. We base our assessment in part on our earlier reports [4-7], where issues of a toroidally-asymmetric divertor biasing have been investigated in the context of the COMPASS-D tokamak.

The main body of this paper is organized in such a way as to allow the reader to quickly assess the proposed experiment on the basis of simple, order-of-magnitude estimates. A more detailed analysis of some particular issues, with lengthy equations, can be found in the appendices.

In all general equations we use the cgs system of units. In "practical" numerical estimates we use mixed units, specified in every case.

2. Typical geometrical and other parameters

MAST is a spherical tokamak, whose typical magnetic configuration is shown in Fig. 2. We will be concerned with the outboard side of the plasma, where the proposed biasing experiment is to be carried out. (This is more practical in MAST than biasing the inner divertor.) Accordingly, in what follows, when using the word "divertor", we will always refer to the outer divertor. The upper and the lower parts of this divertor are symmetric with respect to the horizontal mid-plane. Each divertor target consists of 12 radial carbon "ribs" (Fig. 3), which are 3 cm wide and 20 cm tall. They extend radially from R = 100 cm to R = 166 cm. The instantaneous plasma imprint on the ribs is several times narrower than 66 cm; the reason why the ribs have such large radial extent is that they have to accommodate a broad variety of plasma configurations. Two of the ribs are wider than the others (19 cm instead of 3 cm); an array of flush-mounted Langmuir probes are situated on the upper surface of one of these two ribs, and thermocouples are installed on the other.

The magnetic field in the plane containing the upper faces of the ribs is predominantly toroidal and intersects the surface of the upper faces at a shallow angle $\theta \sim 0.25$ rad, whereas the vertical surfaces are intersected almost normally (at $\pi/2$-θ). The

[1] It is not clear whether convection induced in the region above the X point should necessarily lead to a confinement degradation of the core plasma; on the other hand, the scenario where the convection is limited to the zone below the X point is certainly more attractive in this regard.

magnetic flux (and the plasma flow) is intercepted, therefore, mostly by vertical faces of the ribs. In the proposed experiment, every other rib (6 in total) of the lower divertor will be biased, while the rest of the ribs (6 in total) will remain grounded. The upper divertor will remain grounded. The maximum bias potential will be +100 V.

The divertor geometry and plasma parameters in the SOL vary depending on the tokamak operational regime. For our numerical estimates, we have chosen the following set of parameters, which are representative of the present mode of operation.

1. Toroidal magnetic field strength in the strike zone
$$B_T = 0.2 \text{ T}. \quad (1)$$
2. Poloidal component of the magnetic field in the strike zone
$$B_P = 0.04 \text{ T}. \quad (2)$$
3. Major radius of the separatrix strike point at the outer divertor
$$R = 110 \text{ cm}. \quad (3)$$
4. Vertical extent of the wetted area on each divertor rib,
$$a = \frac{2\pi R}{12}\frac{B_P}{B_T} = 10 \text{ cm}. \quad (4)$$
5. Radial width of the strike zone outside the separatrix
$$b = 6 \text{ cm}, \quad (5)$$
and the same width in the private flux region.
6. Connection length between the lower X-point plane and the divertor surface for the field line that strikes the divertor at a distance b=6 cm from the separatrix
$$L_{\|} = 600 \text{ cm}. \quad (6)$$
7. Plasma density at the divertor target
$$n = 10^{12} \text{ cm}^{-3}. \quad (7)$$
8. Electron temperature
$$T_e = 10 \text{ eV} \quad (8)$$
9. Ion temperature
$$T_i = 60 \text{ eV} \quad (9)$$
The ion temperature is not measured directly but is inferred from the total power balance.
10. Ion and electron gyroradii ($r_{Li,e} = \sqrt{2T_{i,e}/m_{i,e}}/\omega_{Bi,e}$) in a 0.2 T magnetic field
$$r_{Li} = 0.7 \text{ cm}, \; r_{Le} = 0.005 \text{ cm} \quad (10)$$

These parameters have to be considered as "typical" ones, not the ones necessarily met simultaneously in a particular shot.

We assume that the divertor operates in a low-recycling attached mode, so that the parameters of the plasma stream approaching the divertor are determined by sources situated above the X-point.

3. Plasma state prior to biasing

The SOL width b_0 in the zone above the X-point is of the order of 1 cm. Using a standard estimate relating the cross-field diffusion distance within the residence time $L_{\|0}/v_{Ti}$, one finds an estimate of the diffusion coefficient in this zone as $D_0 \sim b_0^2/2(L_{\|0}/v_{Ti})$. (Here $L_{\|0}$ denotes a connection length between the equatorial plane and the vicinity of the

X-point; we recall that $L_{\|}$ is the connection length between the X-point and divertor floor). We use the subscript "0" to designate parameters related to the zone above the X-point. For $L_{\|0}$~10 m and the other parameters as listed above, the resulting diffusion coefficient is

$$D_0 \sim 4 \cdot 10^3 \text{ cm}^2/\text{s}, \tag{11}$$

and corresponds roughly to the diffusion coefficient found in other experiments. As a reference point for the diffusion coefficient, we shall use the Bohm diffusion coefficient,

$$D_{Bohm} = \frac{1}{16}\frac{cT}{eB}, \tag{12}$$

or, numerically,

$$D_{Bohm}(cm^2/s) \approx 600\frac{T(eV)}{B(T)}. \tag{13}$$

Taking $T=T_e$ and B~0.2 T, one finds that $D_{Bohm} \sim 3 \cdot 10^4$ cm^2/s. In other words, D_0 is, roughly speaking, an order of magnitude less than D_{Bohm}, in agreement with other tokamak experiments (e.g., Refs. [8-10]).

The poloidal flux expansion from the equatorial plane to the divertor is about 4. This would lead to a width of the plasma imprint on the divertor plate of the order b~4 cm, which is somewhat less than actually observed (see Eq. (6)). This difference can be explained by cross-field diffusion which occurs during the plasma flight time between the X-point and the divertor. Somewhat puzzling is the significant width of the plasma imprint in the private flux region. Diffusion, with the diffusion coefficient (11), is insufficient to produce a 6 cm wide imprint during the plasma flight-time between the X-point and the divertor floor. This may mean that, for some reason, diffusion in the private flux region is stronger than in the common flux region. Another explanation could be that there is a significant plasma influx from the inner divertor. For the plasma flow from the inner divertor, the connection length is about 10 m, making the discrepancy less acute. Some contribution may also come from the possibly present poloidal electric field and corresponding E×B drift [11].

The ions in the SOL are essentially collisionless. Indeed, their mean free path (for the plasma parameters mentioned in Sec. 2) is

$$\lambda_i \sim 40 \text{ m}, \tag{14}$$

i.e., much longer than the connection length. On the other hand, electrons are collisional, with

$$\lambda_e \sim 1 \text{ m}, \tag{15}$$

Some toroidally asymmetric potential variations can be present in the plasma even in the un-biased case, because of the discreteness of the divertor ribs [1,2] . However, this effect should be small, because all the vertical faces are identical and are intersected by the magnetic field lines at the same, almost 90-degree angle. The horizontal faces intercept a small fraction of the magnetic flux. At any rate, potential variations induced by the varying tilt cannot exceed ~ T_e/e (see Ref. 2), and, as we demonstrate below, this is insufficient to induce noticeable convection.

4. What bias is required to produce a significant broadening?

We shall show in the next few sections that potential perturbations introduced by biasing of the lower divertor ribs can hardly penetrate above the X-point. Therefore, the plasma that enters the zone below the X-point experiences the effect of biasing only during its time of flight to the absorbing surface. We also note that, in the absence of a parallel electric field, the E×B drift keeps the particle trajectory within an equipotential surface. Assuming that the amplitude of potential variations is φ_0 and their spatial scale in the direction perpendicular to the field lines is a yields the following expression for the radial drift velocity:

$$v_D \sim c\frac{\varphi_0}{aB_T}. \tag{16}$$

When making this estimate, we have ignored the radial electric field which generally exists in the SOL. Its role will be discussed later in this section.

One can expect a significant effect of this radial drift if the radial displacement that occurs during the time of flight,

$$t_{\|} = \frac{L_{\|}}{v_{Ti}}, \tag{17}$$

is greater than the radial width of the strike zone, b:

$$v_D t_{\|} > b, \tag{18}$$

or, equivalently,

$$\varphi_0 > \frac{Babv_{Ti}}{cL_{\|}}. \tag{19}$$

We recall that $L_{\|}$ is a connection length between the X-point and the divertor floor. Numerically, for deuterium, Eq. (19) implies

$$\varphi_0(V) > 100\frac{B(T)a(cm)b(cm)\sqrt{T_i(eV)}}{L_{\|}(cm)}. \tag{20}$$

For our representative set of plasma parameters (Sec. 2), this means that φ_0 should exceed a mere 15 V. This estimate is, probably, somewhat pessimistic, because the connection length (6) applies to field lines at a relatively large distance from the separatrix and increases by a factor of 1.5-2 for field lines closer to the separatrix.

Let us now consider the presence of a pre-existing electric field perpendicular to the magnetic flux surfaces. The associated potential difference is typically equal to

$$\varphi_i \sim 3T_i/e. \tag{21}$$

The presence of this radial potential difference makes the equipotentials look as shown in Fig. 4. In the case of a "small" (in a sense defined below) biasing potential the particle displacement normal to the magnetic surface cannot exceed the amplitude of the wiggles of the equipotentials,

$$\delta r \sim \frac{b\varphi_0}{\varphi_1} \tag{22}$$

This estimate holds for δr less than the SOL width ("small" biasing potential) and breaks down when δr becomes greater than b, i.e., when

$$\delta\varphi_0 > \delta\varphi_1 \tag{23}$$

When the condition (23) is satisfied, the wiggles of the SOL exceed its initial thickness; this is a domain where a strong effect of the induced convection can be expected. Numerically, for the reference set of parameters listed in Sec. 2, condition (23) is more restrictive than the condition (20): it yields 30 V instead of 15 V.

As was pointed out in Ref. 1, one can reduce the required potential amplitude compared with the estimate (23) by segmenting the ribs in the radial directions, with bias applied to every second segment. The required potential difference then decreases, roughly speaking, in proportion to the number of segments. However, in the proposed MAST experiment radial segmenting is not anticipated, and one has to use the constraint (23).

Note that the biasing will affect not only the common flux region but also the private flux region. It would be interesting to see if the biasing induces detectable signals at the probes situated in the private flux region near the inner strike point.

5. Shear-flow turbulence

The estimate (16) implied that the potential variation occurs on the scale a which is the poloidal projection of the distance between two neighboring ribs, $2\pi R/12$ (Eq. 5). However, at least in the vicinity of the divertor plates, the potential variation occurs only in narrow region at the interfaces of flux tubes leaning on biased and un-biased ribs (Fig. 5a). The potential gradients (and drift velocities) are very large in these zones, while they vanish in the rest of the flux tube volume. Such a state should, however, give rise to a strong shear flow turbulence, which will smear out the flow over the whole flux tube (Fig. 5b), and smoothen the potential distribution.

Let us evaluate the time required for this smoothening. Imagine a plasma stream of the width x immersed into a plasma at rest (Fig. 6). The characteristic time for development of shear-flow perturbations of a scale Δ (shorter wavelengths can also be unstable but are less efficient in terms of mixing) can be evaluated as (see, e.g., [12])

$$t_{shear} = v_D / \Delta \tag{24}$$

According to the Prandtl theory of a turbulent boundary layer, the broadening of the flow will occur at the rate

$$\frac{1}{\Delta}\frac{d\Delta}{dt} \sim \frac{C}{t_{turb}} \sim \frac{Cv_D}{\Delta}, \tag{25}$$

where C is a numerical constant of the order of 0.3. As $v_D \sim c\varphi_0 / B\Delta$, one finds that x grows according to

$$\Delta^2 \sim 2Cc\varphi_0 t / B \tag{26}$$

where the time is measured from the instant when the plasma flow has entered the zone below the X-point. In order for this flow to encompass the whole thickness of the flux tube within the parallel time of flight (i.e., in order for x to become ~$a/2$), the following condition should be satisfied:

$$\varphi_0 > \frac{Ba^2 v_{Ti}}{8CcL_{\|}}. \tag{27}$$

Numerically, this condition does not differ much from the condition (19) and does not impose any significant new constraints. The ion gyroradius for 60 eV ions in a 0.2 T field is 0.7 cm, i.e., a factor of a few less than the characteristic thickness of the flux tube. With finite-gyroradius effects taken into account, the smoothing should occur even more rapidly.

One has to remember that the unperturbed flow enters the divertor region from the top, where the potential perturbations are already smeared out, and then proceeds towards the plate where one may expect stronger electric fields in the transition zones between the flux tubes leaning on the biased and unbiased ribs. This problem is therefore somewhat different from the one we have discussed above, where the jets are broadening in the y direction while propagating in the z direction. However, the estimate of the characteristic time for the broadening of the shear flow to the size a/2 that follows from Eq. (26) should not depend on this difference.

Also, the model of shear-flow turbulence described by Eqs. (24)-(26) is somewhat oversimplified as it does not take into account the effect of boundary conditions at the underlying conducting plates. For flute-like perturbations, the presence of a conducting boundary may cause a significant reduction of the growth rate for long wavelength modes (see. Ref. 13). In our case, the longest wavelength of interest in the spreading the plasma flow is the wavelength equal to the period of perturbations in the y direction (Fig. 5), i.e., the mode with

$$k=\pi/a \sim 0.3 \text{ cm}^{-1}. \tag{28}$$

Following the analysis of Ref 13, one can show that suppression of this mode does not occur if the following condition is satisfied:

$$\frac{e\varphi_0}{T_i} > \frac{1}{k^4 r_{Li}^3 L_{\|}} \frac{T_i}{T_e}. \tag{29}$$

For the parameters listed in Sec. 2, and k as in Eq. (28), the r.h.s. is equal to approximately 3. In other words, some slowing down of shear-flow instability may occur

for the longest wavelength, if the applied potential is around 60-100 eV. However, for even slightly (by a factor of 1.5) shorter wavelengths, the suppression becomes insignificant.

The other effects not considered in our discussion are the effects of a finite Alfven velocity v_A (finite beta) and of a finite electron thermal velocity v_{Te}. For perturbations with the wave number defined by Eq. (28) the conditions that these effects are insignificant are [14, 15]

$$\frac{e\varphi_0}{T_i} < \frac{v_A}{v_{Ti}} \cdot \frac{1}{k^2 r_{Li} L_\parallel}, \tag{30}$$

and

$$\frac{e\varphi_0}{T_i} < \frac{v_{Te}}{v_{Ti}} \cdot \frac{1}{k^2 r_{Li} L_\parallel}, \tag{31}$$

respectively. Both these conditions are marginally satisfied for the set of plasma parameters presented in Sec. 4. Therefore, one may expect that the modes excited in the biased divertor will differ somewhat from pure flute modes. We leave a detailed analysis of these modes for future publication.

6. Magnetic shear

In the vicinity of the X-point the magnetic field is strongly sheared. The shear causes each flux tube to be squeezed in the radial direction and to be elongated in the poloidal direction. The area of the poloidal cross-section remains nearly constant since the toroidal field strength does not vary much. As a result of the squeezing, the projection of a divertor rib along the magnetic field onto the poloidal plane is distorted and becomes very narrow close to the X-point, see Fig 7. Sufficiently far upstream, its width becomes smaller than the ion gyroradius, which effectively prevents the induced convection from penetrating above the X-point. Indeed, as shown in an appendix, in the X-point region the poloidal wavelength of the biasing electric field is proportional to the distance to the separatrix above the X-point. Since the SOL is only a few cm thick, this implies that, at least as far as the ions are concerned, the biasing voltage probably does not penetrate into the SOL much above the X-point. In fact, solving the equations of motion for an ion as it streams along the magnetic field from the main SOL into the divertor and finally hits the target shows that the "effective time of flight" leading to the radial displacement is equal to that given in Eq (17) with an effective length $L_{//}$ somewhat longer than that used above. The calculation is presented in Appendix 1.

Although the biasing potential perturbations are smaller than the ion gyroradius above the X-point, they could still exist there because of the high mobility of electrons along the magnetic field. If the biasing voltage oscillates with some suitably chosen frequency, it should be possible to detect it in the magnetic midplane using a reciprocating probe. Such an experiment would be of some fundamental plasma physics interest as it would shed light on the physical processes governing electric field penetration into a highly conducting plasma.

7. Effect of the sheath potential

The amplitude of the biasing potential used in the previous sections was related to the potential inside the plasma, not the potential applied to the divertor ribs. Generally speaking, there is a difference between the two caused by the presence of the sheath potential. To evaluate this effect, we use the following model: we assume that on the other side of SOL the plasma leans on a conducting plate which is kept at a constant (ground) potential. This can be thought of as the upper divertor plate; one could also artificially introduce this grounded surface somewhere above the X-point, where the induced potential structures are most probably smeared out by the magnetic shear.

Assume first that the current flows along the magnetic field lines and consider a flux tube of a constant cross-section connecting two electrodes. We shall denote the current as positive if it flows from the biased electrode (on the left) to the grounded electrode (on the right). We neglect potential variations along the flux tube, outside the sheaths (Fig. 8). Simple calculations presented in Appendix 2 show that the current density is

$$j = enu\frac{\exp\left(\frac{e\varphi_b}{T_e}\right)-1}{\exp\left(\frac{e\varphi_b}{T_e}\right)+1} \tag{32}$$

where φ_b is the biasing potential with respect to the ground, u ($\sim v_{Ti}$) is a velocity of the ion flow towards the plate, and φ_b is the current density parallel to the magnetic field lines. The quantity φ_0 that we have introduced in the previous sections is related to φ_b by the equation (see Appendix 2)

$$\varphi_0 = \frac{T_e}{e}\ln\frac{\exp\left(\frac{e\varphi_b}{T_e}\right)+1}{2}. \tag{33}$$

One sees that, for positive φ_b, φ_0 is invariably less than φ_b. The difference is, however, insignificant at biasing potentials exceeding a few T/e. Note also that, by using negative biasing, it is impossible to create a potential modulation exceeding $0.8T/e$ inside the plasma.

Equation (32) shows that the current density does not exceed the ion saturation current even when operating at high positive biasing potentials. This is explained by the fact that, in the case when the cross-section of the current channel is constant, the current is limited by the ion saturation current to the grounded electrode. This is important because, in order to reach potential variations inside a plasma exceeding a few times T/e, we need to introduce a significant positive biasing.

On the other hand, if the current does not flow exactly along the field lines, and can be collected from an area significantly exceeding the area of the positively biased electrodes, the current density on these electrodes may exceed the ion saturation current. To assess this effect in a more quantitative way, we assume that the cross-sectional area of the current channel is different at the left and the right electrodes. Accordingly, instead

of the condition $j_{left}=j_{right}$, one has to use a condition $j_{left}=Aj_{right}$, where $A=S_{right}/S_{left}>1$. This leads to the following modification of Eqs. (32) and (33):

$$j = enu\frac{A\exp\left(\frac{e\varphi_b}{T_e}\right)-A}{\exp\left(\frac{e\varphi_b}{T_e}\right)+A} \tag{34}$$

$$\varphi_0 = \frac{T_e}{e}\ln\frac{\exp\left(\frac{e\varphi_b}{T_e}\right)+A}{A+1} \tag{35}$$

Plots of j and φ_0 vs φ_b are presented in Fig. 9 for various values of the parameter A.

In MAST, if the current flows strictly along magnetic field lines and therefore closes between the biased ribs of the lower divertor and the ribs of the upper divertor (all of which are un-biased), then $A=1$. In the other limiting case, when the currents and potential perturbations do not penetrate above the X-point (see Sec. 9), the current closes between six biased and six unbiased ribs of the lower divertor. Here, again, $A=1$. If one assumes that the current stays within SOL but closes between the six biased ribs and all the unbiased ribs of both the upper and lower divertor (18 in total), then $A=3$. In all these cases, positive biasing leads to no increase or a moderate increase of the current from the biased ribs with respect to the ion saturation current. A significant increase is possible only if the current collected by the biased ribs originates from large surface areas outside the SOL. This does not look very probable in light of experiments on TEXTOR [16] where positive biasing of the limiter (up to 500 V) was not accompanied by any significant increase of the current to it. The current is also limited by a finite plasma resistivity along the current path, the effect that we have ignored, so that equation (35) corresponds to a worst possible case in terms of the current density at positively biased ribs.

8. Additional heating associated with divertor biasing.

The heat flux to the divertor plate surface is equal to [17]

$$q_{left} = nu\left[W_i + e(\varphi_p - \varphi_b) + 2T_e\right] \tag{36}$$

$$q_{right} = nu\left[W_i + e\varphi_p + 2T_e\right] \tag{37}$$

in the case of nearly normal incidence characteristic of the present MAST design. Here W_i is defined so as to make nuW_i equal to the ion energy flux on the plasma side of the sheath. In the unbiased case these fluxes have a common value

$$q^* = nu\left[W_i + \left(\ln\frac{v_{Te}}{2\sqrt{\pi u}} + 2\right)T_e\right] \tag{38}$$

Assuming that the temperatures do not change after the biasing (they are determined by the conditions in the upper part of the SOL, which is not affected by the biasing), and using Eq (A2.4), one finds that

$$q_{left} - q^* = nuT_e \ln \frac{1+\exp(-\frac{e\varphi_b}{T_e})}{2} < 0 \qquad (39)$$

$$q_{right} - q^* = nuT_e \ln \frac{1+\exp(\frac{e\varphi_b}{T_e})}{2} > 0 \qquad (40)$$

Somewhat paradoxically, the heat flux to the positively biased ribs decreases, whereas the grounded ribs experience an increased flux. (This is, in fact, obvious: when we bias a rib positively, the potential difference between it and the plasma decreases, leading to a weaker ion acceleration in the sheath, whereas the electron flux remains, according to equations (A2.1) and (A2.4), essentially unchanged). For $e\varphi_b/T_e=3$ (required to achieve a significant change in the wetting pattern, see Sec. 4), one has $q_{right}-q^* = 2nuT_e/e$. For plasma parameters indicated in Sec. 2, this would mean a relative increase of the heat load by a mere 10%. For $e\varphi_b/T_e=10$, corresponding to 100 V biasing voltage, the relative increase of the heat load on the unbiased ribs is also modest, about 50%.

9. How far upstream do potential perturbations penetrate?

Sustaining convective motion against viscous dissipation requires a current flowing in the plasma and originating at the biased ribs. One might think that Ohmic resistance to this current would lead to a decrease of the potential difference between the neighbouring flux tubes at some distance from the divertor plates. This would then set the length scale for penetration of potential perturbations to the SOL plasma. However, as the analysis presented in Appendix 3 shows, for a low-density SOL plasma typical of current experiments on MAST this process alone is too weak and yields parallel length scales much in excess of the connection length.

A more important factor is flux tube squeezing in the region near the X-point [18]. The distance between equipotentials corresponding to projections of the edges of biased and unbiased ribs becomes very small as one approaches the X-point and reaches the upper SOL, above the X-point (Fig. 2). This increases the role of viscous effects dramatically; in addition, as mentioned in Sec. 7, ion FLR effects become important and, eventually, even electron FLR effects come into play. All this, taken together, makes penetration of potential perturbations above the X-point impossible (for MAST magnetic geometry; however, in the case of "short-legged" divertors of some other tokamaks, this is possible).

10. Discussion

Developing the general theory of induced convection by divertor plate biasing [1,2] and applying this theory to MAST, we have shown that a significant effect of biasing the SOL structure can be expected at relatively small biasing voltages of the order of 30 V. This should lead to large inward-outward radial shifts of wetted zones on the divertor ribs

and, most probably, to the onset of convection. The resulting broadening of the wetted zones would give rise to reduction of the heat flux.

Furthermore, the potential perturbations introduced by the biasing of the lower divertor are expected to be limited to the zone below and near the X-point and thus to be essentially decoupled from the upper part of the SOL surrounding the core plasma. It is therefore quite probable that even a strong biasing will not lead to any confinement degradation of the core plasma.

The current density at the biased plates should not increase much above the ion saturation current even if the bias potential is well above T/e (assuming that the current is closed within the SOL region; if the current is collected from a large area of plasma walls outside the SOL, a significant increase of the current to biased ribs is possible). The biasing and a corresponding redistribution of the energy flux between biased and unbiased plates will result in some decrease of the energy flux to (positively) biased plates and its increase to the unbiased plates.

The slowest time-scale related to establishing of a steady state after some sudden change in plasma parameters is the ion time of flight from the X-point to the divertor target. In MAST, this is about 80 μs, i.e., shorter than a characteristic time of the ELM event. Therefore, one can expect that the biasing will mitigate the heat load enhancement during ELMs.

There should be several effects that could be used to detect the predicted plasma behavior in the MAST SOL. First, the plasma footprint on the divertor ribs will be either shifted inward or outward on the ribs, or broadened (if the convection or some other smoothing mechanism is at work). This can be detected by the electrostatic probes and infrared imaging. Simultaneous imaging of several (both biased and unbiased) divertor ribs could help in distinguishing between these wiggles and general broadening. As the outer divertor ribs cover both the common and private flux regions, some redistribution of the plasma density may occur in the private flux region of the *inner* lower divertor. It might be detectable by the probe array situated on the inner divertor wall.

As indicated in Sec. 5, the biasing should lead to an onset of intense shear-flow turbulence. Characteristic frequencies would vary along the field lines, as the thickness of the shear-flow region between flux tubes leaning on biased and unbiased ribs varies. Halfway between the X-point and the divertor ribs, where $x \sim a/2$ (see Sec. 4 for the definition of x) the frequency should be of the order of $\omega \sim 4c\varphi_0/Ba^2$. For $\varphi_0 \sim$ 30 V, and other parameters as in Sec. 2, this frequency is around $2 \cdot 10^5$ s^{-1} (~40 kHz). Near the ribs, the dominant frequency component would be higher by a factor of 4 to 5.

In addition to serving its primary purpose of spreading the plasma flow over a larger area on the divertor plates, the biasing technique could be used for studying pre-existing plasma turbulence. Generation of shear flow may suppress drift modes initially present in the plasma. This would manifest itself in a change of the fluctuation spectra. (The analysis of this phenomenon is, however, beyond the scope of this paper.)

In closing, we remark that many of the physics issues discussed in this paper are of quite general character, and that our predictions, being based on quite simple and reliable physics, should hopefully be robust.

Acknowledgments

The work by P. Helander was funded jointly by Euratom and the UK Department of Trade and Industry. The work of R. Cohen and D. Ryutov was performed under the auspices of the U.S. Department of Energy at the University of California Lawrence Livermore National Laboratory under contract # W-7405-Eng.-48. The authors thank S. Fielding and G. Counsell for valuable discussions of experimental aspects of the problem. One of the authors (D.R.) is grateful to the Culham Laboratory for its hospitality during the visit associated with this work.

Appendix 1: Particle motion in the biased divertor

In this Appendix, we calculate the net radial drift of a collisionless ion orbit due to divertor plate biasing. This is an extension of the calcuation presented in Ref 7 to MAST geometry. Unlike COMPASS-D, MAST has long divertor legs, and the magnetic field can only be approximated as in Ref 7 close to (within about 20 cm from) the X-point. Instead, the magnetic field must be described by the general formula

$$\mathbf{B} = I\nabla\zeta + \nabla\zeta\times\nabla\psi, \tag{A1.1}$$

where ζ is the toroidal angle, $I = RB_\zeta$ is nearly constant in the divertor region, and ψ is the poloidal flux function. If the electrostatic potential is constant along magnetic field lines, this implies that the usual E×B drift in the ψ-direction is equal to

$$\frac{d\psi}{dt} = c\frac{\mathbf{B}\times\nabla\varphi}{B^2}\cdot\nabla\psi = c\frac{\partial\varphi}{\partial\zeta} \tag{A1.2}$$

and thus remains constant along a field line. In order to obtain the total radial deflection of a particle, we should integrate this expression along a particle orbit,

$$\Delta\psi = \int_{-\infty}^{t_*}\frac{d\psi}{dt}dt, \tag{A1.3}$$

until it hits the target at $t=t_*$. In doing do, it is however important to account for the strong squeezing of the convective cells in the region around the X-point. This makes the electric field vary on the length scale of the gyroradius, which reduces the drift, making the net radial displacement (A1.3) finite. Thus, we write the total radial deflection as a sum of two integrals

$$\Delta\psi = \int_{-\infty}^{t_0}\frac{d\psi}{dt}dt + \int_{t_0}^{t_*}\frac{d\psi}{dt}dt = \Delta\psi_x + \Delta\psi_d, \tag{A1.4}$$

where the first term, $\Delta\psi_x$, describes the contribution from the region above and near the X-point, where the potential perturbations vary on the length scale of the gyroradius, and

the second term, $\Delta\psi_d$, is the contribution from the lower part of the divertor, where the wavelength of the perturbation is longer than the gyroradius and (A1.2) is applicable.

In the first of these regions, toroidal curvature may be neglected, and the magnetic field can be approximated by that close to an X-point in straight field-line geometry, see Ref 7. The field lines are then described by

$$y = d - y_0 e^{R(\zeta-\zeta_0)/L_s}, \tag{A1.5}$$

where the shear length L_s is about 300 cm in MAST, and y is the coordinate along the outer divertor leg, defined so that y=d at the X-point and y=0 at the top of the divertor ribs, see Fig 5. The parameter ζ_0 measures the location where $y=d-y_0$, which can be chosen at will within the X-point region. Because of the turbulent smoothening discussed in Sec. 5, we expect the electrostatic potential to vary approximately sinusoidally with ζ, so that in the X-point region

$$\varphi(y,\zeta) = \varphi_0[1+\sin N\zeta_0(y,\zeta)], \tag{A1.6}$$

$$\zeta_0(y,\zeta) = \zeta - \frac{L_s}{R}\ln\frac{d-y}{y_0}, \tag{A1.7}$$

where N=6 is the number of biased divertor ribs. Close to and above the X-point, i.e., for $d-y<NL_s r_{Li}/R$, the potential varies on the gyroradius length scale and it is not possible to use the usual drift equations to describe the motion. Instead, we observe that since the magnetic field is dominated by its toroidal component, which does not vary much over the gyroradius, the quantity

$$p_x = m_i v_x - eBy/c \tag{A1.8}$$

is a constant of motion on the time scale of the gyromotion; here x is the coordinate perpendicular to y in the poloidal plane, i.e., the radial coordinate. This implies that the guiding-centre drift in the x-direction caused by the presence of the electric field is related to the displacement that this field causes in the average (over a gyroperiod) position in y,

$$\bar{v}_x = \omega_{Bi}(\bar{y} - Y), \tag{A1.9}$$

where $\omega_{Bi} = eB/m_i c$ and $Y = -p_x/m_i\omega_{Bi}$. On the other hand, the motion in the y-direction is governed by the equation

$$\frac{d^2y}{dt^2} + \omega_{Bi}^2(y-Y) = -\frac{e}{m_i}\frac{\partial\varphi}{\partial y} = -\frac{e\varphi_0 NL_s}{m_i R(d-y)}\cos N\left(\zeta - \frac{L_s}{R}\ln\frac{d-y}{x_0}\right), \tag{A1.10}$$

which is obtained by using the constant of motion (A1.8) in the full equations of motion. The average displacement of the particle position caused by the electric field is obtained by integrating this equation along an unperturbed orbit,

$$y = Y + r_{Li} \sin \omega_{Bi} t \tag{A1.11}$$

in the linear approximation. To the lowest order in $r_{Li}/(d-Y)$, this becomes

$$\omega_{Bi}^2 (\bar{y} - Y) = -\frac{e\varphi_0 N L_s}{(d-y) m_i R} J_0\left(\frac{N L_s r_{Li}}{(d-y)R}\right) \cos N\zeta_0 \tag{A1.12}$$

The guiding-centre drift velocity is thus

$$\mathbf{v}_d = -\hat{\mathbf{x}} J_0\left(\frac{k_0 r_{Li} y_0}{d-y}\right) \frac{c}{B} \frac{\partial \varphi}{\partial y}, \tag{A1.13}$$

with $k_0 = NL_s/R$. In other words, the usual E×B drift is reduced by a factor equal to the Bessel function J_0. In the absence of any radial electric field, the phase $N\zeta_0$ of the particle with respect to the biasing stays constant as the particle moves along the magnetic field, while the distance from the X-point increases exponentially,

$$y = d - y_0 \exp\left(\frac{v_{//}(t-t_0)}{L_s}\right), \tag{A1.14}$$

where $v_{//}$ is the parallel velocity. Using these results, we conclude that the net displacement a particle suffers in the region of the X-point is

$$\Delta\psi_x = \int_{-\infty}^{t_0} \frac{d\psi}{dt} dt = c\frac{\partial \varphi}{\partial \zeta} \int_{-\infty}^{t_0} J_0\left(k_0 r_{Li} e^{v_{//}(t_0-t)/L_s}\right) dt = \frac{\partial \varphi}{\partial \zeta} \int_{k_0 r_{Li}}^{\infty} \frac{J_0(u)}{u} du, \tag{A1.14}$$

which for small $k_0\rho$ becomes

$$\Delta\psi_x = c\frac{\partial \varphi}{\partial \zeta} \frac{L_s}{v_{//}} \left(\ln k_0 \rho + \ln 2 - \gamma\right) = c\frac{\partial \varphi}{\partial \zeta} \frac{L_x}{v_{//}}, \tag{A1.15}$$

where $\gamma = 0.577$ is Euler's constant. This defines the "effective length" L_x of the field lines in the X-point region. The total displacement follows by adding the contribution from the lower part of the divertor, $\Delta\psi_d$, Expressed in terms of the broadening at the target, this becomes

$$\Delta x = \frac{\Delta\psi_x + \Delta\psi_d}{RB_p} = -\frac{\pi c \varphi_0 \cos N\zeta}{aB_T} \frac{L_{//}}{v_{//}}, \tag{A1.16}$$

where the total effective length is $L_{//} = L_x + L_d$, with the L_d the length of the field line in the divertor region from x_0 to the target. This estimate of $L_{//}$ exceeds 10 m, suggesting that the number used in the main body of the paper is rather conservative.

As mentioned in Sec. 4, we might expect that a background radial electric field $\mathbf{E}_0 = -\nabla V(\psi)$, with $V(\psi) \approx 3T_e(\psi)$, is present in the SOL. This modifies the drift trajectories in the biased divertor and reduces the radial displacement. The E×B drift assiociated with $\mathbf{E}_0$,

$$c\frac{\mathbf{B}\times\nabla V}{B^2} = cV'(\psi)\left(\frac{I\mathbf{B}}{B^2} - R^2\nabla\zeta\right) \tag{A1.17}$$

makes a particle drift from one convective cell to the next,

$$\frac{d\varphi}{dt} = c\frac{\mathbf{B}\times\nabla V}{B^2}\cdot\nabla\varphi = -cV'(\psi)\frac{\partial\varphi}{\partial\zeta}, \tag{A1.18}$$

Combining this equation with Eq (A1.2), one finds that the total potential φ+V stays constant along the trajectory (as always for E×B drift), and the particle follows the "wiggly" equipotentials discussed at the end of Sec. 4.

Appendix 2: Effect of sheaths on divertor plates

The current densities to the left and the right plates in Fig. 8 are given by the expressions

$$j_{left} = en\left[\frac{v_{Te}}{2\sqrt{\pi}}\exp\left(e\frac{\varphi_b - \varphi_p}{T_e}\right) - u\right] \tag{A2.1}$$

$$j_{right} = en\left[-\frac{v_{Te}}{2\sqrt{\pi}}\exp\left(-e\frac{\varphi_p}{T_e}\right) + u\right] \tag{A2.2}$$

where φ_b is the biasing potential, φ_p is the plasma potential with respect to ground, u is the velocity of the ion flow towards the plate on the plasma side of the sheath, $u \sim v_{Ti}$, and $v_{Te,i} = (2T_{e,i}/m_{e,i})^{1/2}$. From the conditions $j_{left} = j_{right} = j$, one finds the current density and the plasma potential:

$$j = enu\frac{\exp\left(\frac{e\varphi_b}{T_e}\right) - 1}{\exp\left(\frac{e\varphi_b}{T_e}\right) + 1} \tag{A2.3}$$

$$\frac{e\varphi_p}{T_e} = \ln\frac{v_{Te}}{2\sqrt{\pi}u} + \ln\frac{\exp\left(\frac{e\varphi_b}{T_e}\right) + 1}{2} \tag{A2.4}$$

For a flux tube with both ends leaning on the un-biased electrodes, the plasma potential will be equal to the first term on the right-hand side of Eq. (A2.4). Subtracting this potential from that determined by Eq. (A2.4), gives the quantity we have denoted by φ_0 in the main body of the text,

$$\varphi_0 = \frac{T_e}{e} \ln \frac{\exp\left(\frac{e\varphi_b}{T_e}\right)+1}{2}. \qquad \text{(A2.5)}$$

Appendix 3: Penetration of potential perturbations to the upstream plasma

In this Appendix, we start our analysis from a simple model of a uniform magnetic field in the zone below the X-point. After that, at the end of the Appendix, we consider effects caused by magnetic shear.

Consider a "control surface" tangential to the upper surfaces of the divertor ribs (Fig. 5). The magnetic field is directed along the axis z. As in Appendix 1, the coordinate x is an analog of a radial coordinate in the tokamak geometry. The angle θ that determines the tilt of the control surface with respect to the magnetic field is assumed to be small, $\theta << 1$. The distance z_1 along the field lines between this surface and the surface of a rib (Fig. 5) is a few tens of centimeters. We shall show that this distance is much smaller than the distance by which potential perturbations penetrate into the plasma. In this case, the projected potential distribution in the plane perpendicular to the field lines (Fig. 5b) will be essentially the same as the projected potential distribution over the control plane, for several periods in the y direction (defined in Fig. 5). We assume that the potential distribution in the $z=0$ plane is given by

$$\varphi\big|_{wall} = \varphi_0 \cos k_x x \cos k_y y \qquad \text{(A3.1)}$$

The real distribution can be represented by a superposition of such harmonics. We include a radial (x) dependence for generality, to account for possible segmenting of the divertor ribs in the radial direction. In the case of MAST, where the whole rib will be charged to the same potential, one has $k_x << k_y$, whereas the characteristic value of k_y is

$$k_y \sim \frac{N}{\theta R} \sim 0.3 cm^{-1}, \qquad \text{(A3.2)}$$

where N=6 is the number of biased divertor ribs. We emphasize that, in this part of our paper, the magnetic field is assumed to be uniform, in particular, without shear. We also assume that the unperturbed plasma is uniform. This simple model will allow us to identify key physical processes and most important scaling parameters of the problem. After having done that, we will introduce additional effects, e.g., magnetic shear.

According to Eqs. (10) and (A3.2), the product $k_y r_{Li}$ is much less than 1. Because of this, we describe the cross-field plasma motion by a simple hydrodynamic equation,

$$\rho \mathbf{v} \cdot \nabla \mathbf{v} = -\nabla p + \frac{\mathbf{j}_\perp \times \mathbf{B}}{c} + \eta \nabla^2 \mathbf{v} \qquad \text{(A3.3)}$$

where the velocity **v** is just the E×B drift velocity,

$$\mathbf{v} = -c\frac{\nabla\varphi \times \mathbf{B}}{B^2} \tag{A3.4}$$

There is also a parallel flow velocity but it does not enter the problem we are considering. Such a model has been successfully used in the theory of electrostatic probes [18, 19]. Our program is as follows: we find $\mathbf{j}_\perp$ from Eq. (A3.3); then we use the current continuity equation to find the parallel component of the current,

$$\frac{\partial j_z}{\partial z} + div\mathbf{j}_\perp = 0; \tag{A3.5}$$

and finally, we find the potential difference along the field line (including the sheath potential) required to sustain this parallel current; the "penetration length" corresponds to the distance where all the applied voltage is "consumed" by the potential drop along the field line.

As we shall see, the parallel scale L_0 for the potential variation is much larger than the perpendicular scale length. This circumstance allows one to obtain the following simplified expression for j_z

$$\frac{\partial j_z}{\partial z} = \frac{c^2\rho}{B^2}\mathbf{v}\cdot\nabla_\perp\left(\nabla_\perp^2\varphi\right) - \frac{c^2\eta}{B^2}\nabla_\perp^2\left(\nabla_\perp^2\varphi\right) \tag{A3.6}$$

The first term on the rhs is quadratic in φ, cf. Eq. (A3.4), and vanishes if

$$\nabla_\perp\nabla_\perp^2\varphi \parallel \nabla_\perp\varphi. \tag{A3.7}$$

This is the case for systems with high symmetry, like cylindrically-symmetric or planar systems. As electrons are collisional (see Sec. 3), the parallel current is related to the potential variation by an Ohm's law:

$$j_z = -\sigma\frac{\partial\varphi}{\partial z}, \tag{A3.8}$$

where σ is the Spitzer resistivity.

For the moment we assume that the potential variations are small enough, so that one can neglect the first term on the right-hand side of Eq. (A3.6). One then obtains the following equation that determines the potential distribution (and, thereby, the convection pattern) in the bulk plasma:

$$\frac{\partial^2\varphi}{\partial z^2} = -\frac{c^2\eta}{\sigma B^2}\nabla_\perp^2\left(\nabla_\perp^2\varphi\right). \tag{A3.9}$$

In this derivation, we have neglected the Joule dissipation of the cross-field current, for the obvious reason that $j_\perp \sim (1/kL_0)j_z << j_z$. One has

$$\nabla_\perp^2 \varphi = -\left(k_x^2 + k_y^2\right)p, \tag{A3.10}$$

and

$$\frac{\partial^2 \varphi}{\partial z^2} = \frac{c^2 \eta k^4}{\sigma B^2}\varphi \equiv \frac{\varphi}{L_0^2} \tag{A3.11}$$

where

$$L_0 = \frac{B}{ck^2}\sqrt{\frac{\sigma}{\eta}} \tag{A3.12}$$

is the penetration length along the field line and $k^2 = k_x^2+k_y^2$. Note that the ions are essentially collisionless, so that their classical cross-field viscosity is almost zero. However, as was pointed out in Sec. 3, the anomalous cross-field diffusion is significant, with the diffusion coefficient being a fraction of D_{Bohm}. The anomalous kinematic viscosity ν is probably of the same order of magnitude as the diffusion coefficient. Accordingly, we assume that

$$\nu \equiv \frac{\varepsilon}{16}\frac{cT_i}{eB}, \tag{A3.13}$$

with $\varepsilon \sim 0.1$. Eq. (A3.12) then yields

$$kL_0 \sim \frac{4}{kr_{Li}}\left(\frac{\lambda_{ei}}{\varepsilon r_{Li}}\right)^{1/2}\left(\frac{M}{m}\right)^{1/4} \tag{A3.14}$$

For a deuterium plasma with parameters listed in Sec. 2, and assuming that $k \sim 0.3$ cm^{-1}, $\varepsilon \sim 0.1$, one finds that $L_0 \sim 5\cdot 10^5$ cm. This estimate shows that, for parameters typical of the MAST edge plasma, viscous and resistive effects alone do not limit the penetration length in any significant way.

Now consider the role of the magnetic shear. As discussed in Sec 6, it causes squeezing of the cross-section of the flux tube in the radial direction, and stretching in the poloidal direction, with only insignificant variation of the cross-sectional area. For a sufficiently slender flux tube, an initially circular cross-section transforms into an elliptical one [18]. This deformation can be conveniently characterized by the *elongation*, E, of the cross-section, defined as the ratio of the major axis of the ellipse to the radius of an initially (at the divertor plate) cylindrical flux tube.

In the vicinity of the X-point, one can use a simple representation of the poloidal magnetic field simliar to that employed in Appendix 1 (Fig. 9). When one is interested in the behavior of a flux tube in the divertor leg and somewhat above the X-point, one can neglect toroidal effects. In this case, one has the following universal expressions for the components of the poloidal magnetic field:

$$B_\xi = \mu\eta; B_\eta = \mu\xi \tag{A3.15}$$

where the orientation of the coordinate axes is shown in Fig. 9, and μ is a parameter characterizing the poloidal field gradient at the X-point. As we have already mentioned in Appendix 1, in the case of MAST, this approximation is accurate within a poloidal distance of about 20 cm from the X-point. Nevertheless, in this Appendix we will use it for the whole divertor, because it correctly reflects qualitative effects of the magnetic shear. Moreover, as we shall see, these effects are indeed most significant just in the vicinity of the X-point.

For a flux tube whose distance s from the separatrix at the divertor plate is small compared to the distance d from the X-point to the divertor plate (Fig. 9), the following simple expression relates the elongation to the coordinate z along the field line [18]:

$$E = \exp(z / L_s), \tag{A3.16}$$

where

$$L_s = B_T / \mu \tag{A3.17}$$

is the characteristic distance along the field line at which the elongation changes by the order of unity. As has already been mentioned in Appendix 1, L_s is about 300 cm. The distance z^* along a field line between the plate and its closest approach to the X-point (the η=0 plane in Fig. 9) depends on the parameter s defined in Fig. 9 (cf. Ref. 18),

$$\exp(z^* / L_s) = \sqrt{d / s}. \tag{A3.18}$$

Therefore, the elongation in the vicinity of the X-point is

$$E^* = \sqrt{d / s} \tag{A3.19}$$

Eq. (A3.19) shows that the elongation in the vicinity of the X-point depends on the flux surface. As representative of the SOL we may consider a flux tube situated halfway between the separatrix and the outer edge of the plasma. At the point where this flux tube reaches its closest proximity to the X-point, the elongation is about 5. We will use this estimate in what follows. Eq. (A3.18) can be also rewritten as:

$$E = (E^*)^{z / z^*} \tag{A3.20}$$

For our "representative" flux tube z^* is approximately 500 cm.

The presence of a large elongation causes an increase of the local cross-field wave number. One can use the following simple extrapolation for an initially circular (or square) flux tube:

$$\hat{k} = Ek, \tag{A3.21}$$

where k is the wave number near the wall, and $\hat{k}$ is the local value of the wave number (k in our previous notations). Substituting Eq. (A3.21) into Eq. (A3.10), one finds

$$\frac{\partial^2 \varphi}{\partial z^2} = \frac{c^2 \eta k^4 E^4}{\sigma B^2} \varphi. \tag{A3.22}$$

An approximate (WKB-type) solution of this equation is

$$\varphi = \frac{const}{E}\exp\left(-\frac{1}{L_0}\int_0^z E^2 dz\right) \qquad \text{(A3.23)}$$

where L_0 is the length defined in Eq. (A3.12). The potential now decreases much more rapidly with z; for the dependence of Eq. (A3.20), the factor in the exponent of Eq. (A3.23) becomes equal to 1 at

$$z \approx L \equiv \frac{L_s}{2}\ln\frac{2L_0}{L_s} \qquad \text{(A3.24)}$$

For the numerical parameters presented above, this length is L~600 cm.

Depending on whether z determined from Eq. (A3.24) is smaller or greater than the parameter z^* for a certain flux surface, the potential structures disappear below or above the X-point. For the structures to disappear below the X-point, the following inequality should hold:

$$\frac{s}{d} < \frac{L_s}{2L_0} \qquad \text{(A3.25)}$$

For flux surfaces not very close to the separatrix, this inequality does not hold. However, even in this case the potential perturbations penetrate only slightly above the X-point (the dependence on z in Eq. (A3.23) is double-exponential). We thus conclude that the magnetic shear makes it very difficult for the potential perturbations to penetrate above the X-point. If, for some reason, one is interested in providing conditions for that, the best way would be to increase a toroidal period of the perturbations [1,2].

Note also, that, even before the potential perturbations disappear, the width of the flux tubes becomes less than the ion gyro-radius (the effect discussed in Appendix 1), so that the condition $\hat{k}\, r_{Li}>1$ replaces the condition $kr_{Li}<1$ satisfied in the lower part of the divertor. As shown in Appendix 1, this reduces the average radial velocity compared to a simple E×B estimate and, accordingly, reduces the SOL transport.

As we have already mentioned in the Introduction, to cause significant SOL broadening on a relatively short segment of a magnetic field line, one needs to apply high biasing voltages, so that the inertial term (the first term in the r.h.s.) in Eq. (A3.6) becomes dominant, and the sheath boundary condition becomes strongly non-linear. Still, the linear analysis presented above is of interest as it sheds light on the processes governing the penetration of the potential perturbations from the surface of the divertor plate to the bulk of the SOL plasma. Creating small biases on the divertor plates, and making them time-varying (say, sinusoidally) would allow one to detect potential perturbations by probes situated in various parts of the SOL and thereby to test our basic understanding of the physical processes governing its behavior.

References

1. R.H. Cohen and D.D. Ryutov. Nucl. Fusion, **37**, 621 (1997).

2. R.H. Cohen and D.D. Ryutov. Phys. Plasmas, **2**, 2011 (1995).

3. A. Sykes, and the MAST Team. Paper IAEA-CN-77/OV4/1 presented at the 18th IAEA Fusion Energy Conference, Sorrento, Italy, October 4-10, 2000.

4. S.J. Fielding, R.H. Cohen, D.D. Ryutov, and P.Helander. Bull. Am. Phys. Soc, **44**, #7, 275 (1999).

5. P.Helander, S.J. Fielding, R.H. Cohen, and D.D. Ryutov. "Controlling SOL transport by inducing plasma convection." 2000 International Sherwood Fusion Theory Conference, Paper 1D55 (2000).

6. P. Helander, S.J. Fielding, R.H. Cohen, and D.D. Ryutov, Czech. J. Phys. **50**, 1421 (2000)

7. S.J. Fielding, P. Helander, R.H. Cohen, and D.D. Ryutov. J. Nucl. Mater., **290-293**, 859 (2001).

8. G.D. Porter et al., in Plasma Physics and Controlled Nuclear Fusion Research 1994 (Proc. 15th Int. Conf. Seville, 1994), Vol. 3, IAEA, Vienna (1995), 423.

9. F. Wising et al., Contrib. Plasma Phys. **36** (1996) 136.

10. D. Post, et al., in Plasma Physics and Controlled Nuclear Fusion Research 1994 (Proc. 15th Int. Conf. Seville, 1994), Vol. 2, IAEA, Vienna (1995), 561.

11. T.D. Rognlien, G.D. Porter, and D.D. Ryutov, "Influence of ExB and Grad-B Terms in 2-D Edge/SOL Transport Simulations," J. Nucl. Mater., Vol. **266-269**, 654 (1999).

12. L.D. Landau and E.M. Lifshitz, *Fluid Mechanics*, Course of Theoretical Physics, Vol. 6 (Pergamon Press, Oxford, 1987).

13. K.Lotov, D. Ryutov, and J.Weiland. Physica Scripta, **50**, 153 (1994).

14. H.Berk, D. Ryutov, and Yu. A.Tsidulko. JETP Lett., **52**, 23 (1990).

15. H.Berk et al. Nuclear Fusion, **33**, 263 (1993).

16. R.P. Doerner et al., Nucl. Fusion, **34**, 975 (1994).

17. G.D. Hobbs and J.A. Wesson. Plasma Physics, **9**, 85 (1966).

18. D. Farina, R. Pozzoli, and D. Ryutov. Nucl. Fusion, **33**, 1315 (1993).

19. V. Rozhansky, A. Ushakov, and S. Voskoboinikov. Contrib. Plasma Phys. **36**, 391 (1996); Plasma Phys. Reports. **24**, 777 (1998).

20. G.D. Porter and D.D. Ryutov. "Theory of Probe Measurements at the Divertor Plate," 1996 International Sherwood Fusion Theory Conference, Paper 1D31 (1996).

Figure captions.

Fig. 1. Cross-section of a tokamak configuration, with convective cells excited in the lower right divertor leg.

Fig. 2. MAST magnetic configuration. Shown as thick lines in the SOL are the projections along the magnetic field of the top of a divertor rib, following the field around the torus by a toroidal angle equal to multiples of 90°.

Fig. 3. A sketch of the lower divertor, centre post, and vacuum tank of MAST.

Fig. 4 Projection of the equipotentials on the poloidal cross-section of the SOL. The separatrix is a thick line at the left. One can expect a gross change of the SOL structure in the case c, when the swing of equipotentials in the radial direction becomes greater than the initial SOL thickness.

Fig. 5. Turbulent shear flow in the biased divertor: a) The geometry of the system. Divertor ribs are shown in thick lines; biased ribs are shown in grey. The wetted areas are of height a (Eq.(4)). Dotted lines represent magnetic field lines tilted by an angle $\theta=B_p/B_T$ with respect to a "control surface" (shown as a dashed line) passing through the top of the divertor ribs. The x-axis is directed away from the reader. b) The potential distribution in the direction y. Solid line – without turbulent smoothening; dashed line – with turbulent smoothening. The period is equal to $a\cos\theta \approx a$ and is shown not to scale with Figure 5a.

Fig. 6. A set of initially narrow jets located in the zones of highest potential gradient near the boundaries of flux tubes leaning on the biased and un-biased ribs (solid lines); and a smooth velocity profile established as a result of turbulent mixing (dashed line).

Fig. 7. Magnetic field in the vicinity of the X-point. Shown in red is the separatrix; d is the distance between the X-point and the control surface of Fig. 5; $s<<d$ is the distance of a certain flux surface from the separatrix near the control surface. Shown as dashed lines are projections of the wetted surface of a certain divertor rib onto the poloidal plane at increasing toroidal distances [6]. Normalizing the length of the green segment to its initial value (near the divertor plate), one finds the quantity called "elongation" (Appendix 3).

Fig. 8. The potential distribution along a current channel of constant cross-section. The solid curve corresponds to the potential distribution without biasing (both end plates grounded); the dashed curve corresponds to the left plate biased to the potential φ_b. The plasma potential, φ_p, is different for the biased and un-biasesd case.

Fig. 9. Plots of a) current density j, and b) plasma potential φ_0 vs biasing potential φ_b. The potentials are normalized to the electron temperature. A is the ratio between the areas of the negative and positive electrodes.

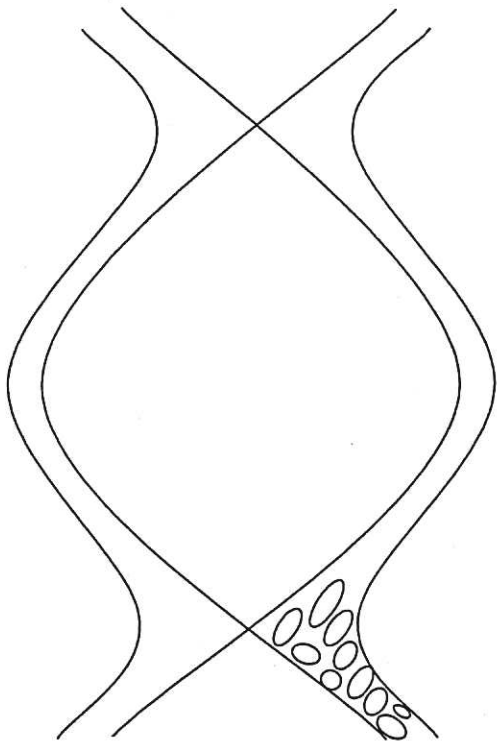

Fig. 1. Cross-section of a tokamak configuration, with convective cells excited in the lower right divertor leg.

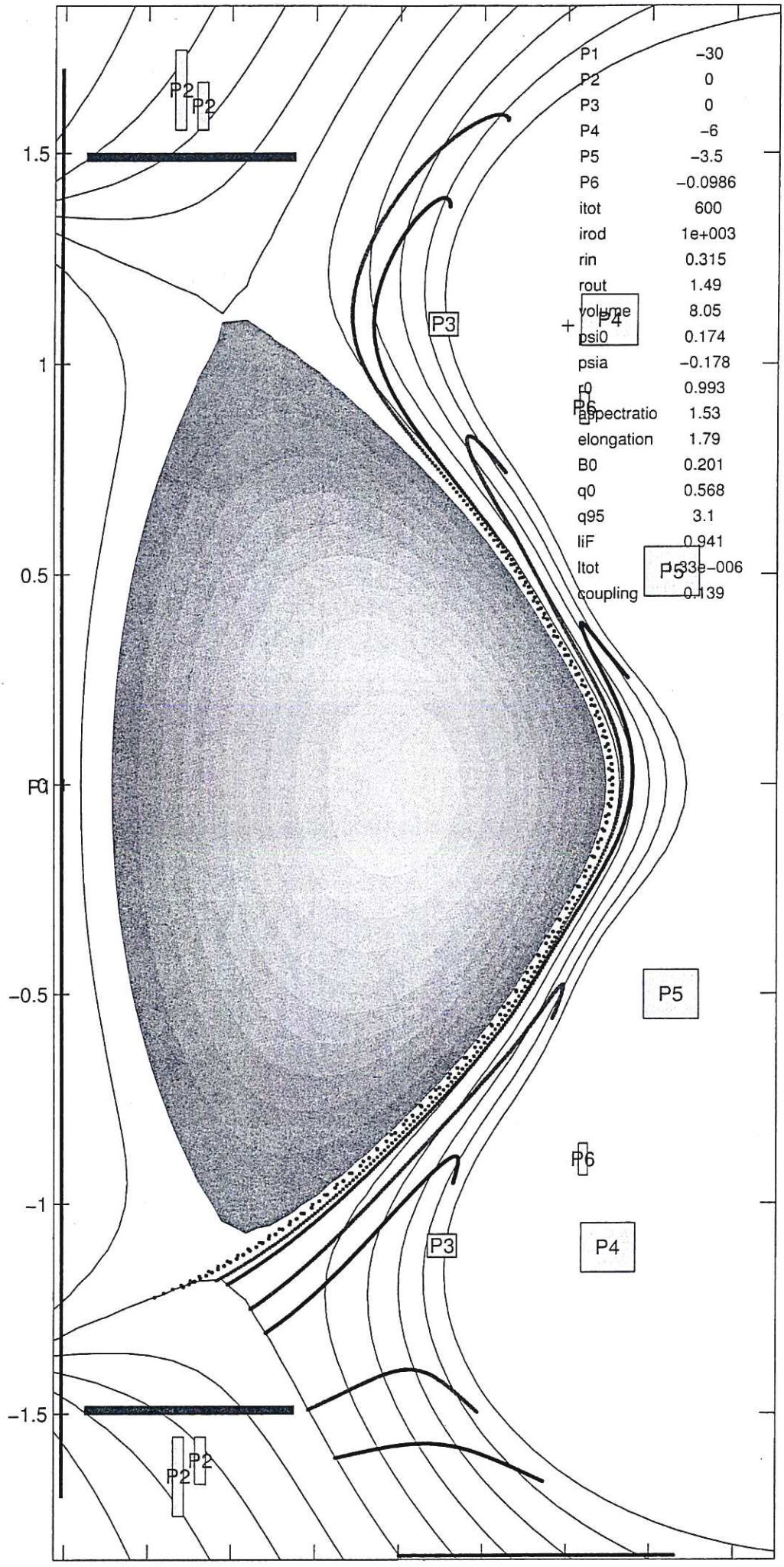
P1 -30
P2 0
P3 0
P4 -6
P5 -3.5
P6 -0.0986
itot 600
irod 1e+003
rin 0.315
rout 1.49
volume 8.05
psi0 0.174
psia -0.178
r0 0.993
aspectratio 1.53
elongation 1.79
B0 0.201
q0 0.568
q95 3.1
liF 0.941
Itot 3.33e-006
coupling 0.139
P1
P2
P2
P3
P4
P5
P6
P3
P2
P2
1.5
1
0.5
0
-0.5
-1
-1.5

Fig. 2

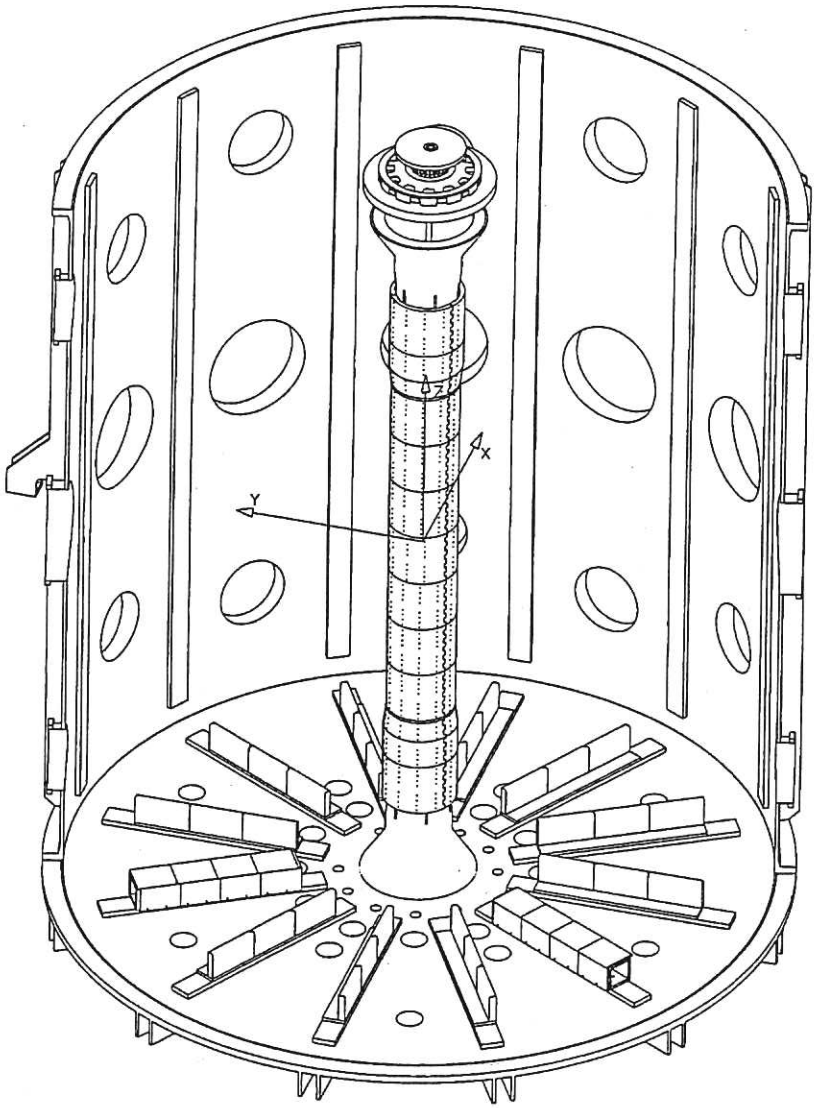

Fig. 3. A sketch of the lower divertor, centre post, and vacuum tank of MAST.

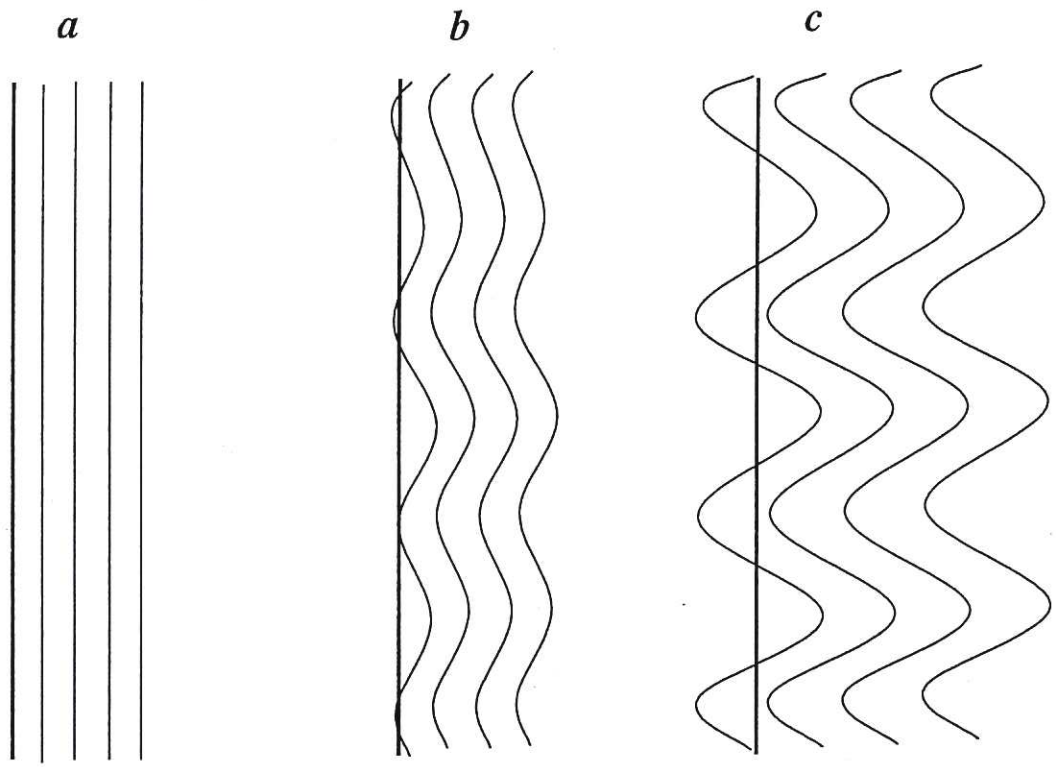

Fig. 4 Projection of the equipotentials on the poloidal cross-section of the SOL. The separatrix is a thick line at the left. One can expect a gross change of the SOL structure in the case c, when the swing of equipotentials in the radial direction becomes greater than the initial SOL thickness.

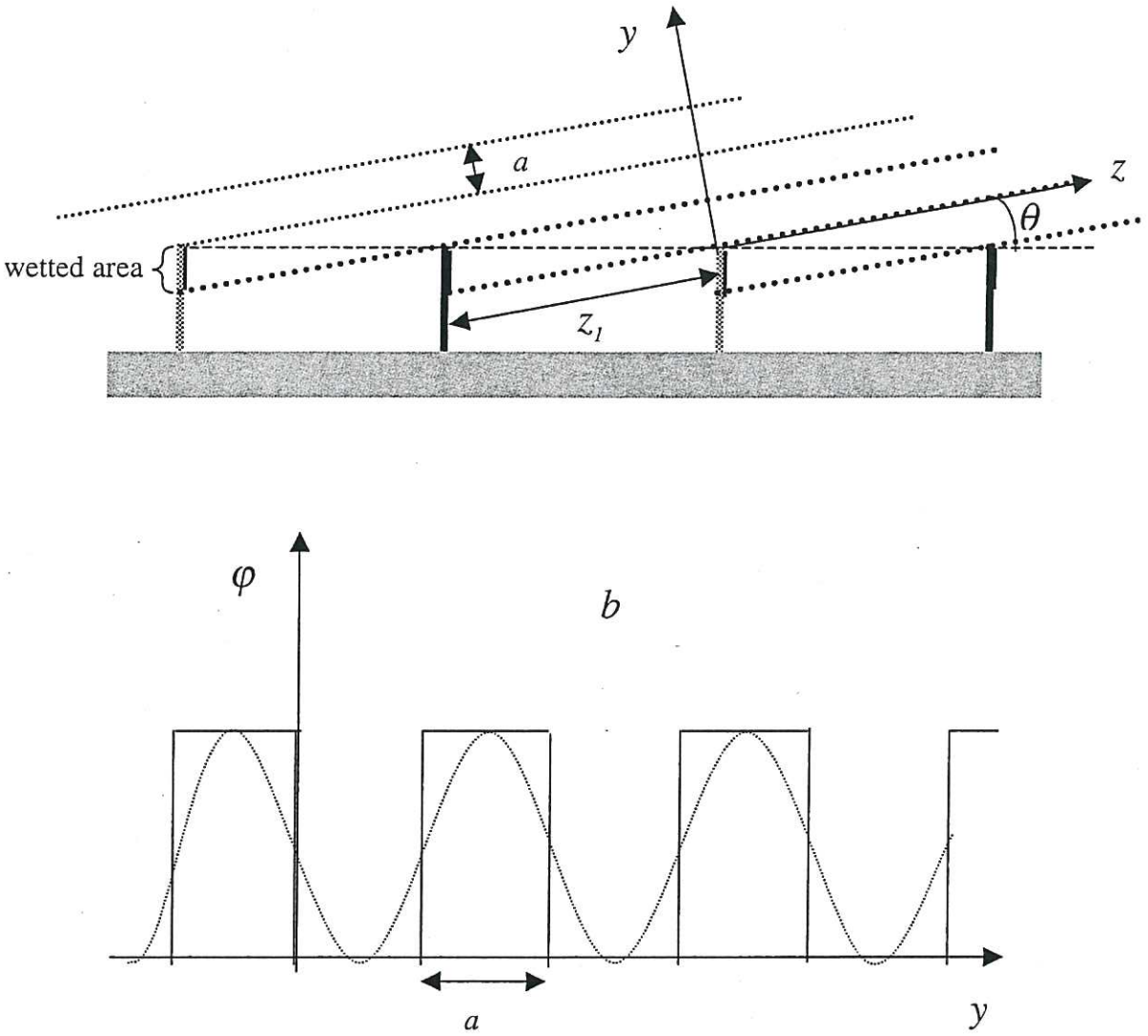

Fig. 5. Turbulent shear flow in the biased divertor: a) The geometry of the system. Divertor ribs are shown in thick lines; biased ribs are shown in grey. The wetted areas are of height a (Eq.(4)). Dotted lines represent magnetic field lines tilted by an angle $\theta=B_P/B_T$ with respect to a "control surface" (shown as a dashed line) passing through the top of the divertor ribs. The x-axis is directed away from the reader. b) The potential distribution in the direction y. Solid line – without turbulent smoothening; dashed line – with turbulent smoothening. The period is equal to $a\cos\theta \approx a$ and is shown not to scale with Figure 5*a*.

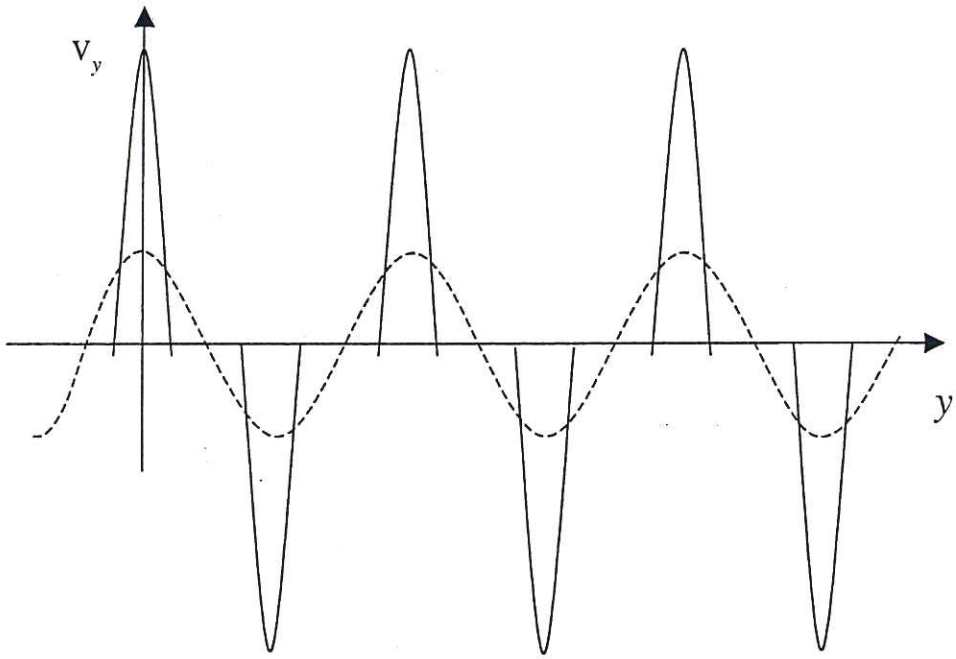

Fig. 6. A set of initially narrow jets located in the zones of highest potential gradient near the boundaries of flux tubes leaning on the biased and un-biased ribs (solid lines); and a smooth velocity profile established as a result of turbulent mixing (dashed line).

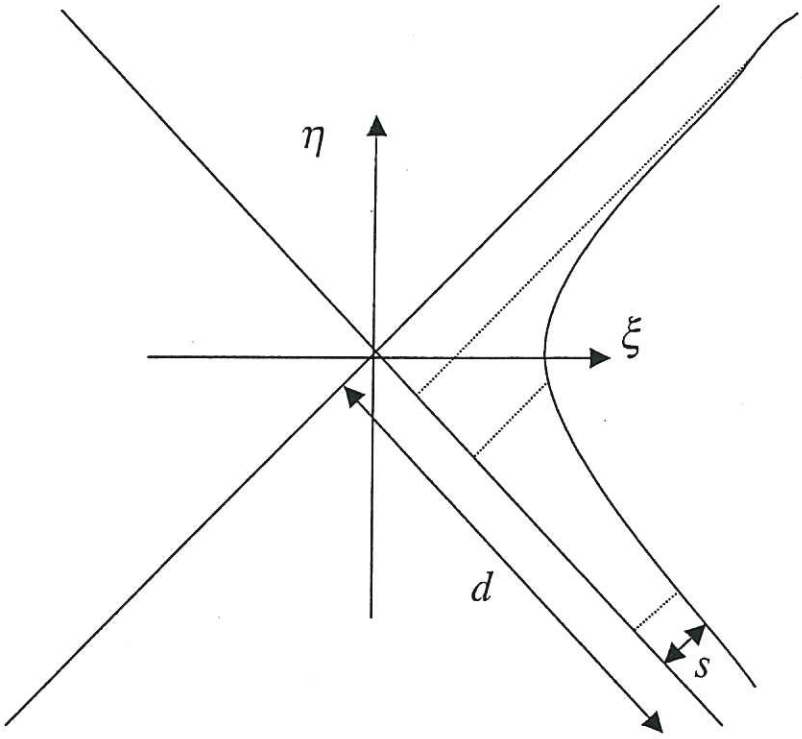

Fig. 7. Magnetic field in the vicinity of the X-point. Shown in red is the separatrix; d is the distance between the X-point and the control surface of Fig. 5; $s<<d$ is the distance of a certain flux surface from the separatrix near the control surface. Shown as dashed lines are projections of the wetted surface of a certain divertor rib onto the poloidal plane at increasing toroidal distances [6]. Normalizing the length of the green segment to its initial value (near the divertor plate), one finds the quantity called "elongation" (Appendix 3).

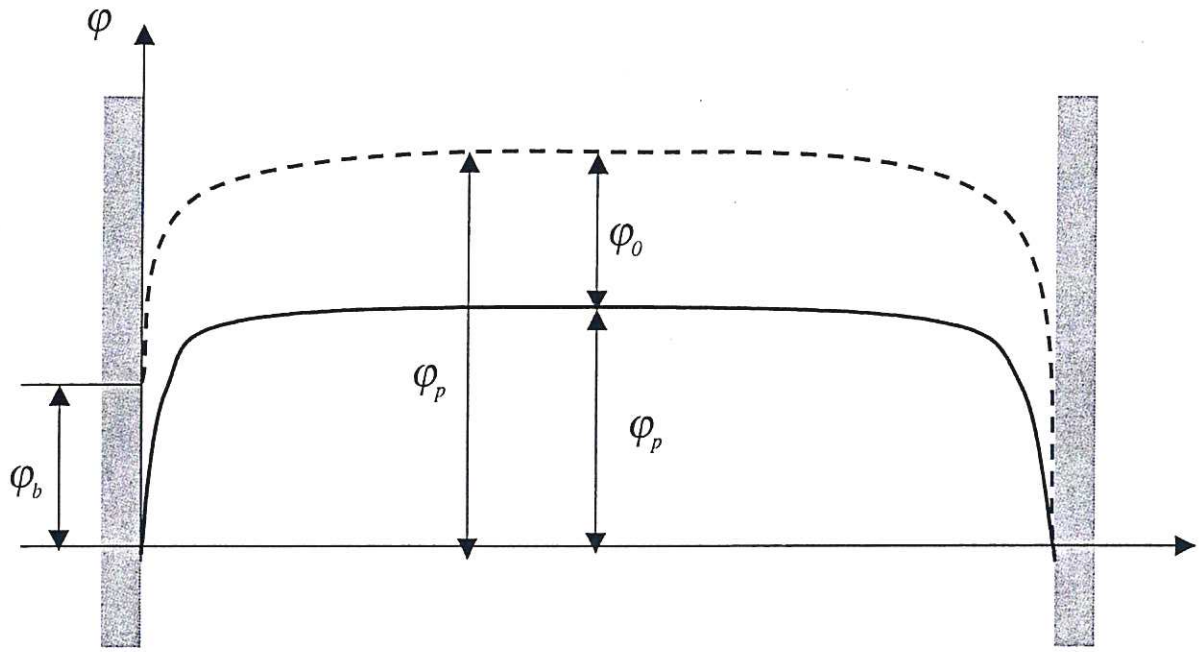

Fig. 8. The potential distribution along a current channel of constant cross-section. The solid curve corresponds to the potential distribution without biasing (both end plates grounded); the dashed curve corresponds to the left plate biased to the potential φ_b. The plasma potential, φ_p, is different for the biased and un-biasesd case.

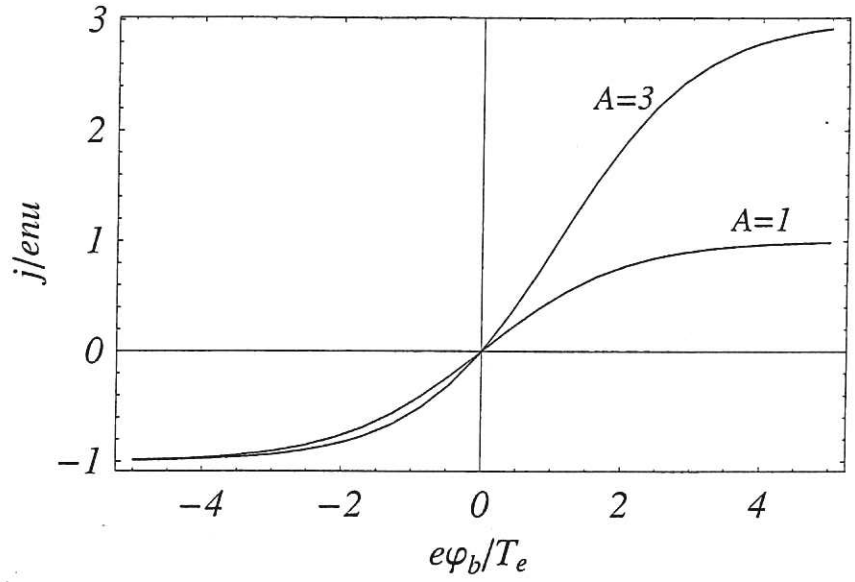

(a)

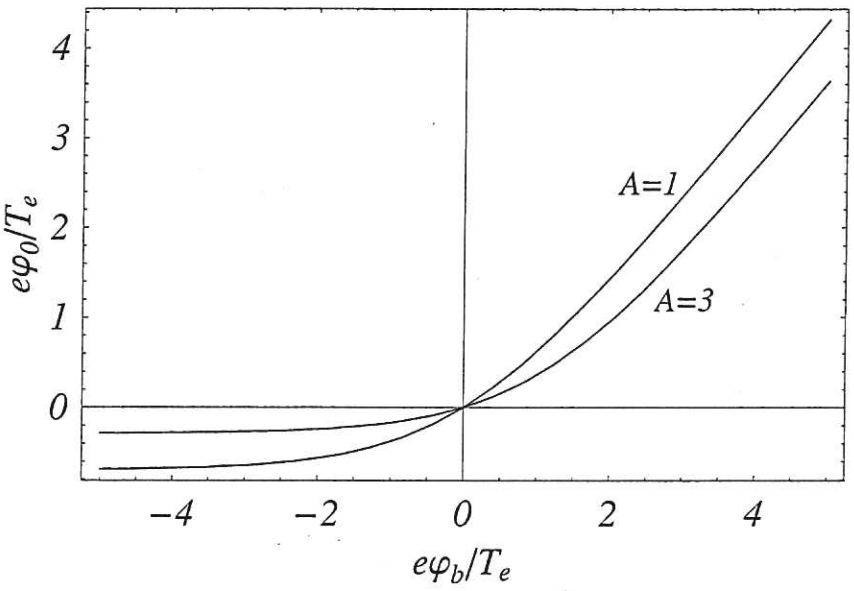

(b)

Fig. 9. Plots of a) current density j, and b) plasma potential φ_0 vs biasing potential φ_b. The potentials are normalized to the electron temperature. A is the ratio between the areas of the negative and positive electrodes.